ChemComm

COMMUNICATION

View Article Online
View Journal | View Issue

Cite this: *Chem. Commun.*, 2024, **60**, 14101

Received 6th August 2024,
Accepted 28th October 2024

DOI: 10.1039/d4cc03994g

rsc.li/chemcomm

GeSe/WSe_2 mixed dimensional p–n junction photoelectric properties†

Bing Yan, *[a] Guoxin Zhang,[bc] Xuan Shi[bc] and Hongquan Zhao [bc]

Heterojunctions prepared utilizing diverse 2D materials enhance a variety of optoelectronic devices. Here, we present GeSe/WSe_2 mixed-dimensional p–n heterojunctions, which broaden the possibility of material combination and selection in 2D/layered heterojunction devices, while also providing material parameters to facilitate the development of optoelectronic devices based on 2D/layered semiconductor materials.

Novel 2D/layered semiconductor materials with graphene-like structure show great potential for development and application in next-generation optoelectronic devices due to many unique and excellent physical and structural properties.[1–3] Van der Waals (VdW) heterojunctions formed by superposition of two or more 2D layered semiconductors through vdW force bonding make it possible for researchers to integrate different materials without having to consider lattice mismatches between materials.[4] The diversity and uniqueness of 2D material properties promotes the diversity of heterojunction device performance.[5,6] Taking full advantage of the properties of each 2D or layer material to construct vdW heterojunctions with excellent performance is expected to lead to the discovery of more novel and unique physical phenomena. This can provide a broad opportunity for fundamental research of 2D materials in the field of optoelectronics and the development and application of next-generation high-performance optoelectronic devices, *e.g.*, photodetectors, transistors and photovoltaic devices, *etc.*[7–9]

Various vdW heterojunctions have been prepared by combining different two-dimensional layered materials through fixed-point transfer or direct growth, including WSe_2/MoS_2,[10] GaTe/MoS_2,[11] WSe_2/SnS_2,[5] MoS_2/WSe_2/EG,[12] *etc.*, revealing their potential for photovoltaics or photodetection. The differences and excellent attributes of 2D materials in terms of bandgap, spin–orbit coupling and work function make vdW heterojunctions have unique properties.[8,13] Based on this, novel optoelectronic devices with unique functionalities have been prepared, including high-performance field effect transistors, tunneling transistors, photodetectors, solar cells, light-emitting diode devices, sensors and storage devices.[6,13–16] The research studies of heterojunction devices with different combinations of 2D materials are fundamental and necessary to advance the development of photodetection. With the development of layered semiconductor materials, the study of mixed-dimensional heterojunctions is gradually emerging.[17,18] The effectiveness of vdW interactions between semiconductors of different dimensions will undoubtedly further expand the possibility of constituting heterojunctions.

Transition Metal Chalcogenides (TMDCs) were some of the first 2D materials to come into the researchers' view and are currently the most widely studied new 2D material system.[19–23] Among them, WSe_2 has attracted much attention due to its tunable bandgap (1.20–1.63 eV), strong light–matter interaction, excellent photoconductivity, layer-dependent photoelectronic and spintronic properties, unique phonon–exciton interaction, and excellent flexibility.[21,24,25] Besides, GeSe, as the most representative semiconductor of group IV–VI, shows a high absorption coefficient of 10^5 cm^{-1} in the visible region,[26] a broad-spectrum optical response of 400–1400 nm,[27] a tunable effective electron mass of 0.03–0.61 m_0,[28] and a high electron mobility of 2.93×10^4 cm^2 V^{-1} s^{-1},[29] which make it attractive and valuable for applications in optoelectronic devices. Chemical vapor deposition (CVD), as a highly controllable and practical growth method for the preparation of 2D materials, has the advantages of fast growth rate, high quality and large deposition area, which is advantageous in the production of high-performance and multifunctional 2D materials.[30] The preparation of monolayer WSe_2 materials with carrier mobility greater than 100 cm^2 V^{-1} S^{-1} has been realized based on the CVD method.[31] In addition, the mechanical stripping method has been widely used to prepare high-quality 2D materials. Due

[a] *School of Physics and Engineering, Henan University of Science and Technology, Luoyang 471023, China. E-mail: 9906383@haust.edu.cn*
[b] *Chongqing Institute of Green and Intelligent Technology, Chinese Academy of Sciences, Chongqing 400714, China*
[c] *Chongqing School, University of Chinese Academy of Sciences, Chongqing 400714, China*

† Electronic supplementary information (ESI) available. See DOI: https://doi.org/10.1039/d4cc03994g

to the weak vdW forces in layered materials, the separation of 2D layered materials is easier to achieve by external forces. At present, this method is still the main way to prepare high-quality single-crystal 2D materials.

WSe_2 2D materials are prepared on a 300 nm SiO_2/Si substrate using a double-temperature zone sliding tube furnace based on CVD. Se powder is used as the precursor, and WO_3 is used as the tungsten source. The Se powder and WO_3 are put into the quartz tubes of the first and second temperature zones of the dual-temperature zone slide tube furnace, respectively (ESI†). To ensure the simultaneous optimization of both the size and quality of the WSe_2, we fine-tuned key growth parameters, including reaction temperature, reaction time, carrier gas flow rate, and the ratio of selenium and tungsten precursors (ESI†). This resulted in large (up to 100 μm), regular triangular crystals with smooth surfaces and well-defined edges. A schematic diagram of the CVD system, the temperature curves of the growth process of WSe_2 materials, and a schematic diagram of the optical microscope morphology and crystal structure are shown in Fig. 1(a)–(d).

GeSe films in GeSe/WSe_2 p–n junctions were obtained from single crystals of GeSe bulk materials (HQ graphene). By employing optimized polydimethylsiloxane (PDMS) with the precise composition and viscosity as the transfer medium, and leveraging an optical microscope and a three-axis micrometer stage, we achieved success in transferring the GeSe thin film, obtained through mechanical exfoliation, onto the WSe_2 two-dimensional material, through meticulous temperature control during the microzone drying and transfer process (ESI†). Similar techniques have been reported in the literature.[32] The GeSe/WSe_2 p–n heterojunction preparation process is shown in Fig. 2(a), the Au electrodes are prepared by laser direct writing, magnetron sputtering and stripping technology (ESI†). The heterojunction devices are annealed under vacuum at 240 °C for 1 h to improve the contact between the GeSe/WSe_2 interface and the electrodes. Schematic diagrams and optical microscope images of a GeSe/WSe_2 mixed-dimension p–n junction before and after GeSe transfer are shown in Fig. 2(b)–(e). The Atomic Force Microscope (AFM) test results in Fig. 2(f) and (g) show the thicknesses of representative areas of WSe_2 and GeSe within the dashed boxes from Fig. 2(e). The thicknesses of WSe_2 and GeSe are 1.06 nm and 365.59 nm, respectively, corresponding to the positions indicated by the upper dashed lines in Fig. 2(f) and (g).

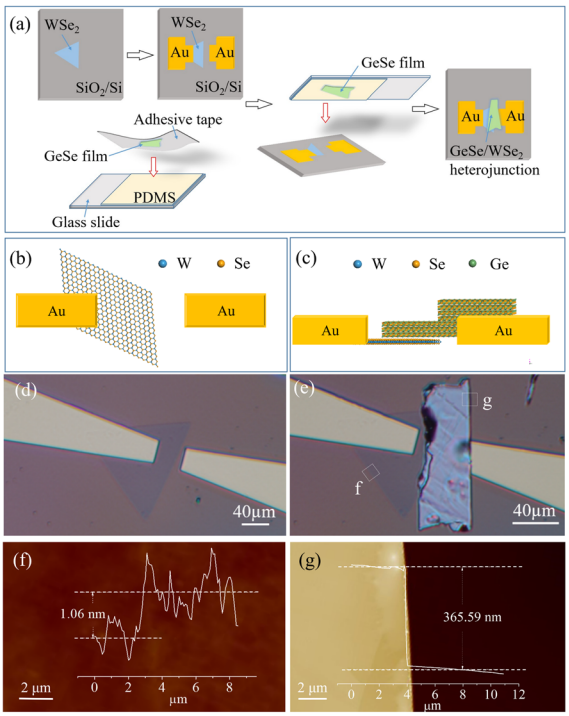

Fig. 2 (a) Schematic diagram of the steps for manufacturing the GeSe/WSe_2 vertical heterojunction by a micro-area dry transferring method. Schematic diagram of the sample (b) before and (c) after GeSe transfer, and optical microscope image of the sample (d) before and (e) after GeSe transfer. AFM images of the (f) WSe_2 and (g) GeSe in the heterojunction.

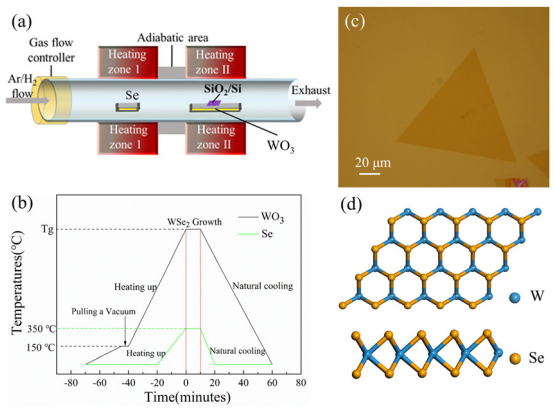

Fig. 1 (a) Schematic diagrams of the CVD system. (b) Growth process temperature curve of WSe_2 material. (c) Optical microscope morphology image of WSe_2 2D material. (d) Crystal structure of WSe_2 2D material viewed from the top and side.

The Raman spectra of GeSe and WSe_2 in the GeSe/WSe_2 heterojunction, depicted in Fig. 3(a) and (b) respectively, are sharp and well-defined, indicating minimal broadening due to lattice defects or disorder. Among them, the three Raman peaks of GeSe located near 80 cm^{-1}, 149 cm^{-1} and 181 cm^{-1} correspond to A_{1g}, B_{3g} and A_{3g} modes,[33] respectively. WSe_2 Raman spectra contain two first-order modes A_1', E′, one phonon mode LA(M) and a series of second-order modes, such as LA(M) + TA(M), which are in agreement with literature reports.[21] The mode in the WSe_2 Raman spectra comes from the transverse vibration of Se–Se atoms and the E′ mode comes from the longitudinal vibration of W–Se atoms (Fig. 3(c)).[34] The LA(M) mode, a longitudinal phonon at the M symmetry point, typically activated by lattice structure disorder,[35] is present but relatively weak, suggesting limited disorder and good lattice quality. Fig. 3(d) shows the photoluminescence (PL) spectra of the WSe_2 2D material under 532 nm laser irradiation at room temperature (RT) and its Gauss–Lorentz curve fitting results. The PL spectra of WSe_2 show peaks for the neutral exciton X and negatively charged exciton X−, indicating clear energy levels and band structure with minimal broadening,[36]

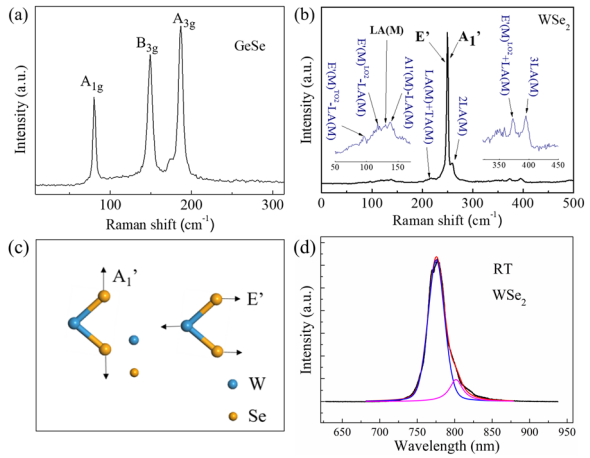

Fig. 3 Raman spectra of (a) GeSe and (b) WSe_2 under the 532 nm laser, (c) first-order Raman vibration modes of WSe_2, and (d) PL spectra of WSe_2 2D material under 532 nm laser illumination at room temperature.

reflecting good crystal quality. Despite unintentional n-type doping in monolayer WSe_2,[37] two fitted PL peaks reveal fundamental exciton transitions and provide insights into the electronic structure. Specifically, short-wavelength peaks are from X, while long-wavelength peaks are from X−, with X− electrons originating from shallow donor ionization.[36] As WSe_2 is a direct bandgap semiconductor with K-point transitions, both X and X− exciton peaks arise from direct K → K transitions.

In order to explore the photoelectric properties of the GeSe/WSe_2 mixed dimensional p–n heterojunction, photoelectricity tests of the heterojunction are performed under 635 nm laser irradiation with an excitation power density in the range of 4.1–28.4 mW cm^{-2}; the spot size of the laser is about 25 mm^2. Fig. 4(a) shows the *I–V* characteristic curves of the GeSe/WSe_2 p–n heterojunction under different power densities. The non-smoothness of the *I–V* curves under a high voltage may be due to small currents in 2D/layered materials, voltage source instability, and amplified noise/electromagnetic interference. The inset shows the *I–V* curves of the heterojunction in the dark, which exhibit obvious rectification characteristics. The current I_{DS} is about 7.5 nA at 3 V and only about 0.5 nA at −3 V. The I_{DS} of the heterojunction device increases from 7.5 nA to 13.1 nA at 3 V with increasing excitation power density. According to eqn (1):

$$R_\lambda = I_{ph}/P{\cdot}S \quad (1)$$

(P is the laser power density and S is the effective area under laser illumination), the evolution of photoresponsivity (R_λ) with laser power density is obtained, as shown in Fig. 4(b). The decrease of R_λ with laser power is a phenomenon common to many photodetectors. It can be attributed to the absorption saturation of the heterojunction and the increase of surface composite processes.

To further explore the stability of the GeSe/WSe_2 heterojunction devices, photo-switch characteristics of the GeSe/WSe_2 heterojunction photodetectors under 635 nm laser irradiation are examined.

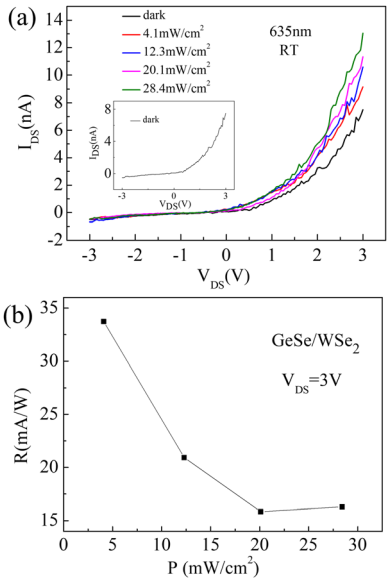

Fig. 4 (a) *I–V* characteristic curves of a GeSe/WSe_2 heterojunction under different laser power densities of 635 nm; the inset shows an *I–V* characteristic curve of the device in the dark. (b) The evolution of R_λ of a GeSe/WSe_2 heterojunction with laser excitation power density.

Fig. 5 shows the time dependence of the I_{DS} under a power density of 28.4 mW cm^{-2} at 3 V. It can be seen that the I_{DS} of the GeSe/WSe_2 heterojunction varies rapidly and consistently over cycles, reflecting a good stability. Fig. 5 shows the time dependence of the I_{DS} under different power densities of a 635 nm laser at 3 V. It is apparent that the I_{DS} varies rapidly and consistently at any power densities by repetitive laser switching. The specific detectivity (D^*) and external quantum efficiency (EQE) are obtained from the following equations:

$$D^* = \frac{R_\lambda \cdot \sqrt{S}}{\sqrt{2eI_{dark}}} \quad (2)$$

$$EQE = \frac{h \cdot c \cdot R_\lambda}{e \cdot \lambda} \quad (3)$$

where S is the effective area irradiated by the laser, e is the electron charge, h is the Planck constant, and c is the light

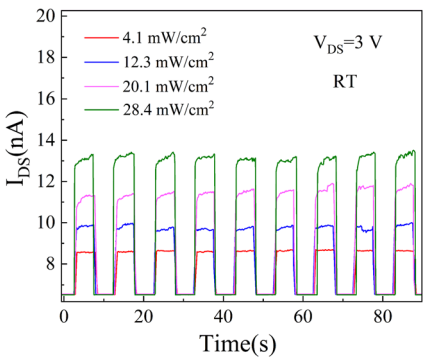

Fig. 5 Optical switching behavior of a GeSe/WSe_2 heterojunction *vs.* different laser power densities with a fixed bias of 3 V.

Table 1 Comparison of important performances of this work to those of other reported heterojunction photodetectors

Materials	Wavelength (nm)	R_λ (mA W^{-1})	EQE (%)
p-WSe_2/n-MoS_2[6]	532	10	2.4
p-GaSe/n-InSe[8]	410	21	9.3
p-GeSe/n-MoS_2[9]	532	105	24.2
p-BP/n-ReS_2[15]	1550	1.8	0.14
p-$MoTe_2$/n-MoS_2[16]	800	38	6
p-GeSe/n-WSe_2 (our work)	635	33.73	65.98

velocity. Based on the photoelectric test results of GeSe/WSe_2 heterojunction devices, the R_λ, D^* and EQE are calculated to be 33.73 mA W^{-1}, 2.39 $\times$ 10^7 jones and 65.98%, respectively, at a laser power density of 4.1 mW cm^{-2} and a bias voltage of 3 V. A comparison between the parameters in this work and the results reported in the literature is presented in Table 1.

In summary, p-GeSe/n-WSe_2 mixed dimensional vertical vdW p–n heterojunction devices are prepared by transferring exfoliated GeSe films onto CVD-grown WSe_2 2D materials. Several critical parameters reflecting the photoelectric properties of GeSe/WSe_2 heterojunctions are obtained, including: photoresponsivity (33.73 mA W^{-1}), specific detectivity (2.39 $\times$ 10^7 jones) and external quantum efficiency (65.98%). The results have expanded the scope of material combinations and selections for two-dimensional/layered heterojunction devices, while offering material parameters for the advancement of optoelectronic devices and demonstrating their high potential in fields such as photodetectors.

This work was supported by the National Natural Science Foundation of China (Grant No. 12304446)

Data availability

Data for this article, including the dataset are available at Science Data Bank at **https://doi.org/10.57760/sciencedb.11252**.

Conflicts of interest

There are no conflicts to declare.

References

1 A. Thakur and B. Anasori, *Science*, 2024, **383**, 1182–1183.
2 J. W. Wang, L. Q. He, Y. H. Zhang, H. Y. Nong, S. N. Li, Q. K. Wu, J. Y. Tan and B. L. Liu, *Adv. Mater.*, 2024, **36**, 23.
3 M. J. Dai, X. R. Zhang and Q. J. Wang, *Adv. Funct. Mater.*, 2024, **34**, 21.
4 H. W. Guo, Z. Hu, Z. B. Liu and J. G. Tian, *Adv. Funct. Mater.*, 2020, **31**, 2007810.
5 T. F. Yang, B. Y. Zheng, Z. Wang, T. Xu, C. Pan, J. Zou, X. H. Zhang, Z. Y. Qi, H. J. Liu, Y. X. Feng, W. D. Hu, F. Miao, L. T. Sun, X. F. Duan and A. L. Pan, *Nat. Commun.*, 2017, **8**, 1906.
6 C. H. Lee, G. H. Lee, A. M. van der Zande, W. C. Chen, Y. L. Li, M. Y. Han, X. Cui, G. Arefe, C. Nuckolls, T. F. Heinz, J. Guo, J. Hone and P. Kim, *Nat. Nanotechnol.*, 2014, **9**, 676–681.
7 J. Su, G. D. Li, X. H. Li and J. S. Chen, *Adv. Sci.*, 2019, **6**, 1801702.
8 F. G. Yan, L. X. Zhao, A. L. Patanè, P. A. Hu, X. Wei, W. G. Luo, D. Zhang, Q. S. Lv, Q. Feng, C. Shen, K. Chang, L. Eaves and K. Y. Wang, *Nanotechnology*, 2017, **28**, 27LT01.
9 Y. Xin, X. Wang, Z. Chen, D. Weller, Y. Wang, L. Shi, X. Ma, C. Ding, W. Li, S. Guo and R. Liu, *ACS Appl. Mater. Interfaces*, 2020, **12**, 15406.
10 J. Wong, D. Jariwala, G. Tagliabue, K. Tat, A. R. Davoyan, M. C. Sherrott and H. A. Atwater, *ACS Nano*, 2017, **11**, 7230–7240.
11 S. X. Yang, C. Wang, C. Ataca, Y. Li, H. Chen, H. Cai, A. Suslu, J. C. Grossman, C. B. Jiang, Q. Liu and S. Tongay, *ACS Appl. Mater. Interfaces*, 2016, **8**, 2533–2539.
12 Y. C. Lin, R. K. Ghosh, R. Addou, N. Lu, S. M. Eichfeld, H. Zhu, M. Y. Li, X. Peng, M. J. Kim, L. J. Li, R. M. Wallace, S. Datta and J. A. Robinson, *Nat. Commun.*, 2015, **6**, 7311.
13 X. Zhou, X. Z. Hu, J. Yu, S. Y. Liu, Z. W. Shu, Q. Zhang, H. Q. Li, Y. Ma, H. Xu and T. Y. Zhai, *Adv. Funct. Mater.*, 2018, **28**, 1706587.
14 S. Q. Zhang, R. Z. Xu, N. N. Luo and X. L. Zou, *Nanoscale*, 2021, **13**, 1398–1424.
15 W. Zhu, X. Wei, F. Yan, Q. Lv, C. Hu and K. Wang, *J. Semicond.*, 2019, **40**, 092001.
16 A. Pezeshki, S. H. Shokouh, T. Nazari, K. Oh and S. Im, *Adv. Mater.*, 2016, **28**, 3216.
17 J. J. Tao, J. B. Jiang, S. N. Zhao, Y. Zhang, X. X. Li, X. S. Fang, P. Wang, W. D. Hu, Y. H. Lee, H. L. Lu and D. W. Zhang, *ACS Nano*, 2021, **15**, 3241–3250.
18 D. D. Xie, L. B. Wei, M. Xie, L. Y. Jiang, J. L. Yang, J. He and J. Jiang, *Adv. Funct. Mater.*, 2021, **31**, 2010655.
19 M. Z. Xu, H. J. Ji, M. W. Zhang, L. Zheng, W. W. Li, L. Luo, M. D. Chen, Z. Liu, X. T. Gan, X. W. Wang and W. Huang, *Adv. Mater.*, 2024, **36**, 19.
20 D. S. Tsai, K. K. Liu, D. H. Lien, M. L. Tsai, C. F. Kang, C. A. Lin, L. J. Li and J. H. He, *ACS Nano*, 2013, **7**, 3905–3911.
21 R. Chaurasiya, A. Dixit and R. Pandey, *Superlattices Microstruct.*, 2018, **122**, 268–279.
22 W. S. Xu, D. C. Kozawa, Y. Q. Zhou, Y. Z. Wang, Y. W. Sheng, T. Jiang, M. S. Strano and J. H. Warner, *Small*, 2019, **16**, 1905985.
23 W. Ding, L. Hu, J. M. Dai, X. W. Tang, R. H. Wei, Z. G. Sheng, C. H. Liang, D. F. Shao, W. H. Song, Q. N. Liu, M. Z. Chen, X. G. Zhu, S. L. Chou, X. B. Zhu, Q. W. Chen, Y. P. Sun and S. X. Dou, *ACS Nano*, 2019, **13**, 1694–1702.
24 L. P. Xu, J. X. Zhou, Z. He, J. B. Hu and M. R. Liu, *Mater. Lett.*, 2021, **284**, 128994.
25 T. J. Wang, K. Andrews, A. Bowman, T. Hong, M. Koehler, J. Q. Yan, D. Mandrus, Z. X. Zhou and Y. Q. Xu, *Nano Lett.*, 2018, **18**, 2766–2771.
26 D. J. Xue, S. C. Liu, C. M. Dai, S. Y. Chen, C. He, L. Zhao, J. S. Hu and L. J. Wan, *J. Am. Chem. Soc.*, 2017, **139**, 958–965.
27 H. Zhao, Y. Yang, C. Wang, D. H. Zhou, X. Shi, Y. Z. Li and Y. L. Mao, *ACS Appl. Mater. Interfaces*, 2019, **11**, 38031–38038.
28 R. X. Fei, W. B. Li, J. Li and L. Yang, *Appl. Phys. Lett.*, 2015, **107**, 173104.
29 Z. Y. Hu, Y. C. Ding, X. M. Hu, W. H. Zhou, X. C. Yu and S. L. Zhang, *Nanotechnology*, 2019, **30**, 252001.
30 A. Thangaraja, S. M. Shinde, G. Kalita and M. Tanemura, *Mater. Lett.*, 2015, **156**, 156–160.
31 J. Chen, B. Liu, Y. P. Liu, W. Tang, C. T. Nai, L. J. Li, J. Zheng, L. B. Gao, Y. Zheng, H. S. Shin, H. Y. Jeong and K. P. Loh, *Adv. Mater.*, 2015, **27**, 6722–6727.
32 L. Wang, I. Meric, P. Y. Huang, Q. Gao, Y. Gao, H. Tran, T. Taniguchi, K. Watanabe, L. M. Campos, D. A. Muller, J. Guo, P. Kim, J. Hone, K. L. Shepard and C. R. Dean, *Science*, 2013, **342**, 614–617.
33 X. Zhou, X. Hu, B. Jin, J. Yu, K. L. Liu, H. Q. Li and T. Y. Zhai, *Adv. Sci.*, 2018, **5**, 1800478.
34 H. Terrones, E. Del Corro, S. Feng, J. M. Poumirol, D. Rhodes, D. Smirnov, N. R. Pradhan, Z. Lin, M. A. T. Nguyen, A. L. Elías, T. E. Mallouk, L. Balicas, M. A. Pimenta and M. Terrones, *Sci. Rep.*, 2014, **4**, 4215.
35 A. Berkdemir, H. R. Gutierrez, A. R. Botello-Mendez, N. Perea-López, A. L. Elías, C. I. Chia, B. Wang, V. H. Crespi, F. López-Urías, J. C. Charlier, H. Terrones and M. Terrones, *Sci. Rep.*, 2013, **3**, 1755.
36 Y. B. Gong, Q. Zhou, X. L. Huang, B. Han, X. P. Fu, H. X. Gao, F. F. Li and T. Cui, *Chem. Nano. Mater.*, 2017, **3**, 238–244.
37 C. R. Zhu, K. Zhang, M. Glazov, B. Urbaszek, T. Amand, Z. W. Ji, B. L. Liu and X. Marie, *Phys. Rev. B: Condens. Matter Mater. Phys.*, 2014, **90**, 161302.

